Appl. Phys. B 78, 315–320 (2004)
DOI: 10.1007/s00340-004-1405-x

Applied Physics B
Lasers and Optics

Y. LI[1]
T. IDO[1]
T. EICHLER[2,*]
H. KATORI[1,2,✉]

Narrow-line diode laser system for laser cooling of strontium atoms on the intercombination transition

[1] Cooperative Excitation Project, ERATO, Japan Science and Technology Corporation (JST), 4-1-8 Hon-cho, Kawaguchi, Saitama 332-0012, Japan
[2] Engineering Research Institute, The University of Tokyo, Bunkyo-ku, Tokyo 113-8656, Japan

Received: 29 September 2003
Published online: 11 February 2004 •

ABSTRACT We report a diode laser system developed for narrow-line cooling and trapping on the $^1S_0$–$^3P_1$ intercombination transition of neutral strontium atoms. Doppler cooling on this spin-forbidden transition with a line width of $\Gamma/2\pi = 7.1$ kHz enables us to achieve sub-μK temperatures in a two-step cooling process. The required reduction of the laser line width to the kHz level was achieved by locking the laser to a tunable Fabry–Pérot cavity. The long-term drift (> 0.1 s) of the reference cavity was compensated by employing the saturated absorption signal obtained from Sr vapor in a heat pipe of novel design. We demonstrate the potential of the system by performing spectroscopy of Sr atoms confined to the Lamb–Dicke regime in a one-dimensional optical lattice.

PACS 32.80.Pj; 39.30.+w; 42.55.Px

1 Introduction

Laser-cooled alkaline-earth atoms are considered as promising candidates for neutral atom based optical frequency standards [1–4], but are also suitable for establishing new paths to create quantum degenerate gases in the 'scalar' $^1S_0$ ground state [5, 6], as well as in the long-lived metastable states $^3P_2$ [7–9] and $^3P_0$. While the $^1S_0$–$^3P_1$ intercombination transitions of alkaline-earth atoms such as Mg [10] and Ca [2, 3, 11] are extensively studied for optical frequency standards, these narrow transitions with line width Γ have also been discussed to lead to efficient laser cooling down to ultra-low temperatures of $k_B T \sim \hbar\Gamma$, yielding minimum temperatures in the range of μK and far below [12, 13]. The recent demonstration of narrow-line Doppler cooling and trapping on the $^1S_0$–$^3P_1$ intercombination transition in ^{88}Sr down to the photon recoil limit has opened a new frontier of sub-μK temperatures for alkaline-earth atoms [14, 15]. Laser cooling on narrow transitions has also been realized in Yb (an alkaline-earth-like atom) [16] as well as in Ca [11]. Recently, the implementation of narrow-line cooling in ^{87}Sr enabled the achievement of two times the Fermi temperature [17], demonstrating an alternative approach for degenerate Fermi systems.

In this paper, we describe a laser system designed for trapping and cooling Sr atoms on the intercombination line. In order to demonstrate the stability of our laser system, we performed Doppler and recoil-free spectroscopy of Sr atoms cooled and trapped in the Lamb–Dicke regime [18] provided by an optical lattice, where the Stark-shift perturbation exerted by the confining optical potential is carefully eliminated using a 'Stark shift cancelation technique' [19, 20].

Strontium has two cooling transitions built on its $^1S_0$ ground state (Fig. 1). The $(5s^2)$ $^1S_0$–$(5s5p)$ $^1P_1$ transition has a natural line width of $\Gamma_B = 2\pi \times 32$ MHz; hence the photon scattering rate is sufficient to capture and cool Sr atoms from oven temperature (400–500 °C) down to the Doppler temperature of $T_D \approx 1$ mK. In order to reach down to ultra-low temperatures we employ the spin-forbidden intercombination line $(5s^2)$ $^1S_0$–$(5s5p)$ $^3P_1$, which exhibits a natural line width of $\Gamma_R = 2\pi \times 7.1$ kHz, in a second cooling stage. Despite its narrowness, the radiation pressure from this transition is sufficiently large to counteract gravity, and therefore enables us to laser cool and magneto-optically trap atoms. Simply by

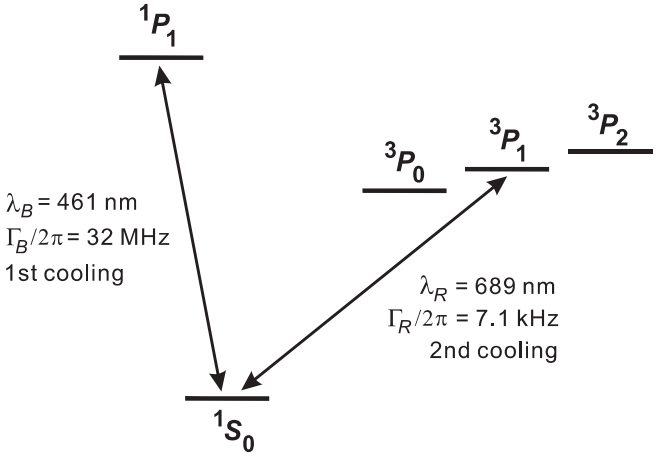

FIGURE 1 Energy levels of strontium relevant for laser cooling. Sub-μK temperatures can be achieved by a two-stage cooling cycle, precooling on the $^1S_0$–$^1P_1$ transition and subsequent narrow-line cooling on the $^1S_0$–$^3P_1$ intercombination transition

✉ E-mail: katori@amo.t.u-tokyo.ac.jp
*Present address: NTT Basic Research Laboratories, 3-1 Morinosato-Wakayama, Atsugi, Kanagawa 243-0198, Japan

Doppler cooling we can easily obtain dense atomic samples at sub-μK temperatures [14]. A crucial point in cooling experiments is the spectral width and the frequency stability of the cooling laser, which should be reduced to the order of the transition line width, i.e. to the kHz regime in the case of the intercombination transition. A standard approach to obtain sub-kHz-stability lasers is to lock the laser frequency to a high-finesse Fabry–Pérot cavity made of ultra-low-expansion glass and minimize the long-term drift of the cavity resonance by stabilization to the zero-expansion temperature [21, 22]. However, in this case the tunability is limited since it is not possible to continuously tune the whole free spectral range of the cavity (typically 1–1.5 GHz) with a single acousto-optic modulator (AOM).

In the search for a simple system with good frequency tunability, we employed a tunable Fabry–Pérot cavity that has two piezo-electric transducer (PZT) disks inserted between an invar spacer and the cavity mirrors. This design enables us to compensate the slow drift of the cavity length by electronic feedback to the PZT by using the error signal obtained from saturated absorption spectroscopy of Sr vapor. We devised a heated absorption cell that provides an error signal with high signal-to-noise ratio to stabilize the laser frequency. In order to examine the performance of the laser system we conducted high-resolution spectroscopy of Sr atoms trapped in an optical lattice.

2 Laser system

2.1 *Extended cavity diode laser*

Our laser system is based on an anti-reflection (AR)-coated laser diode with center wavelength at 685 nm (Hitachi HL6738MG, $P = 35$ mW). The free-running line width of the solitary laser diode (typically tens of MHz) is substantially reduced by employing an extended cavity diode laser (ECDL) setup [23] in Littman–Metcalf configuration [24]. In this design, the output facet of the laser diode is AR coated and the reflecting surface is replaced by an external mirror resulting in a total cavity length of 12 cm. The AR coating raises the lasing threshold of the solitary laser diode from 50 to 75 mA. The output beam is collimated by an AR-coated aspherical lens (Thorlabs LT230, $f = 4.5$ mm, NA $= 0.55$) and diffracted by a holographic grating (Optometrics, 2400 grooves/mm) in grazing-incidence configuration. While the zero-order diffraction constitutes the output beam (about 20% of the diode output), the first-order diffraction is retroreflected by a mirror into the laser diode's waveguide structure. This mirror selects the wavelength which is optically fed back into the laser diode and can be tuned by a PZT actuator. In order to reduce mode hopping as the laser is frequency scanned, the pivot point is located close to the optimum position at the intersection of three lines: the surface plane of the mirror, the grating, and the facet of the diode. If the tuning mirror is well adjusted, the grating dispersion tracks the cavity mode [25]. Our ECDL is temperature stabilized to $T = 30.5\,^{\circ}$C and generates $P = 2$ mW of output light at $\lambda_R = 689$ nm with an injection current of $I \approx 65$ mA. Scanning ranges up to 20 GHz are achieved without mode hops.

2.2 *Frequency stabilization to a tunable Fabry–Pérot cavity*

Feedback by the cavity grating reduces the short-term line width of the free-running diode laser to the 100-kHz level. However, vibration and acoustic noise usually broaden the line width to the MHz regime. In order to further reduce the spectral line width of the ECDL to less than the line width of the intercombination transition (7.1 kHz), the laser was actively stabilized to a tunable high-finesse Fabry–Pérot cavity by employing a frequency modulation (FM) sideband (Pound–Drever–Hall) technique [26]. The optical stabilization scheme is shown in Fig. 2. After traversing a 60-dB Faraday isolator and a cylindrical lens pair to compensate the beam

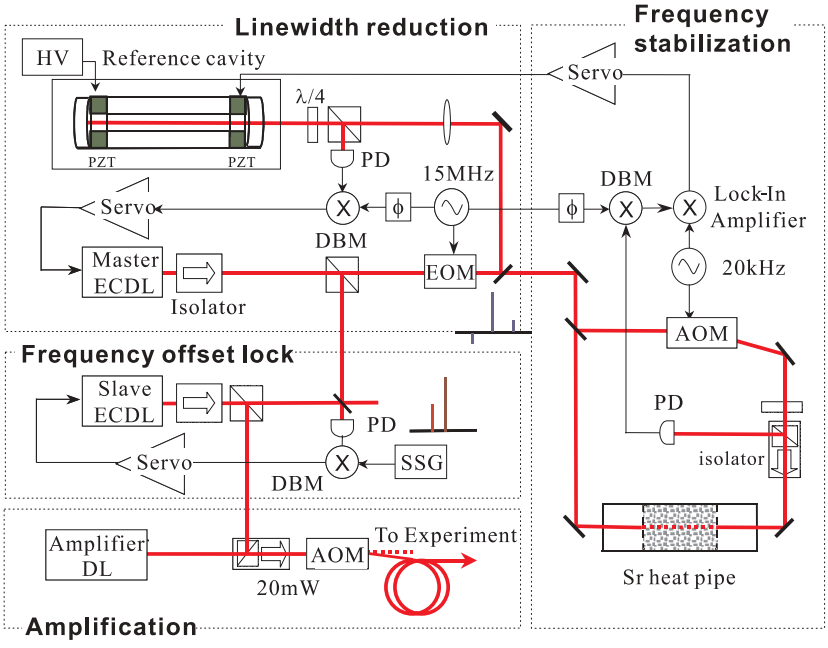

FIGURE 2 Schematic diagram of the laser system's building blocks: line-width reduction by stabilization to a reference cavity, absolute frequency stabilization by Sr saturation spectroscopy, frequency tuning by offset locking to the master laser, and a separate stage for power amplification. The paths of the laser beams and the electric signals are distinguished as *thick lines* and *thin lines*, respectively. Photodiode (PD), double-balanced mixer (DBM), acousto-optic modulator (AOM), high-voltage source (HV), signal generator (SSG)

shape and astigmatism of the laser diode, about 500 μW of the ECDL (master) output is mode matched to the Fabry–Pérot cavity. The laser light is phase modulated by an electro-optic modulator (EOM) operated at a modulation frequency of $f_{RF} = 15.16$ MHz. The reflected light from the cavity is separated from the incoming light by using a $\lambda/4$ wave-plate in combination with a polarizing beam splitter and detected by a Si PIN photodiode (PD). After demodulation of the photodiode signal in a double-balanced mixer, the low-frequency part is amplified, integrated, and fed back to the ECDL via two channels of the electrical servo circuit: a slow feedback loop (< 10 Hz) – driving the PZT of the ECDL mirror – adjusts the laser frequency to a reference cavity resonance. Fast frequency fluctuations are compensated by superimposing the feedback signal onto the laser current, obtaining a total servo bandwidth exceeding 1 MHz. The frequency fluctuation of the stabilized ECDL relative to the center of the cavity resonance was estimated to be about 100 Hz by measuring the noise spectrum of the error signal [27].

Our reference cavity (see upper left in Fig. 2) in non-confocal configuration is composed of a cylindrical super-invar spacer (outer diameter 50 mm) with a length of 100 mm, two PZT disks (Fuji Ceramics C-91) of 2-mm thickness – which are attached to both ends of the spacer – and two high-reflecting ($R \approx 99.97\%$) concave mirrors (radii of curvature 1000 mm, Research Electro-Optics). By applying voltage to the PZT disks, the relative spacing of the mirrors can be controlled. The finesse was measured by cavity-ring-down spectroscopy [28]. From the photon lifetime in the cavity of $\tau = 2.40$ μs, we could infer a finesse of $\mathcal{F} = 11\,300$. The cavity is suspended in a vacuum chamber using molybdenum wires in order to isolate the cavity from mechanical and acoustic vibrations at frequencies over 100 Hz. In addition, the chamber is embedded in quartz sand to attenuate low-frequency acoustic vibrations [29]. The chamber is evacuated to a pressure below 10^{-5} Pa by an ion pump. Thermal stabilization is achieved by servo controlling the chamber temperature.

One of the essential features of our cavity, which facilitates the design of the electronic stabilization circuit, is the use of two separately addressable PZT disks. In order to achieve a stability of 1 kHz combined with a scanning range of a whole free spectral range (FSR) of 1.45 GHz, one needs a relative voltage precision on the order of $10^{-6} = 1\frac{\text{kHz}}{\text{GHz}}$. Although one piezo disk is sufficient to allow for tunability, in practice it is difficult to construct a high-voltage amplifier that has a dynamic range of 120 dB with a 100-Hz feedback bandwidth. We therefore separated the PZT voltage into a high-voltage DC offset channel and a feedback-correction channel which are individually fed to the PZT disks of each of the cavity mirrors. One of them is used for wide-range tuning (1 FSR) and driven by a high-voltage source (HV) for the coarse offset voltage. Its voltage noise is reduced to less than 250 μV by using a low-pass filter that has its −3 dB cut-off frequency at 2 Hz. The second piezo disk serves as compensation of the thermal drift of the cavity for the low-voltage servo loop with a scan range of only 1 MHz. Hence an amplifier with 60-dB dynamic range is sufficient to achieve a frequency stability of 1 kHz. Since the tuning characteristic of the cavity–PZT system is 4 MHz/V, a stability of 1 kHz implies a required voltage accuracy below 250 μV. We were able to reduce the noise to less than 200 μV, which corresponds to laser-frequency fluctuations of 800 Hz, by using low-noise operational amplifiers to drive the PZT in the feedback channel.

2.3 *The strontium cell: novel design*

The stabilization of the laser frequency to a high-finesse reference cavity reduces the laser line width to the 100-Hz level. However, thermal effects give rise to a drift of the reference cavity resonance frequency. To ensure long-term absolute frequency stability, which is crucial for cooling and trapping experiments, we compensate this drift by locking the cavity resonance frequency to the center of the ^{88}Sr atomic resonance.

As reference to compensate the drift of the cavity length we employ saturation spectroscopy of the $^1S_0 - ^3P_1$ transition in Sr vapor. Owing to the very weak oscillator strength, production of a sufficiently high density alkaline-earth metal vapor is required in order to obtain a good absorption signal. In contrast to heavy alkali atoms such as Cs and Rb, the room-temperature vapor pressure of alkaline-earth atoms is two orders of magnitude lower. In order to attain a vapor pressure of $p \approx 10^{-2}$ Pa, corresponding to a number density of $n \approx 10^{12}$ cm^{-3}, the confining vapor cell has to be operated at $T \approx 400$ °C. Such high temperatures put some constraints on the materials used for the vapor cell and the high-vacuum equipment. A further complication associated with alkaline earths is their high corrosive property, i.e. they chemically react with silicates rather easily. At the necessary high operating temperature ordinary quartz windows would quickly blacken and therefore severely limit the lifetime of such a vapor cell. In addition, continuous high-temperature exposure of the copper gaskets to the aggressive alkaline-earth metal vapor must be minimized to avoid vacuum breakdown. Here, we present a simple yet durable novel cell design in which the Sr vapor is confined by windows made of sapphire [30], which does not react with Sr.

The strontium absorption cell is divided into three regions as illustrated in Fig. 3: the central 'vapor cell' of cylindrical shape with dimensions ∅27 mm × 60 mm which contains the Sr vapor, and two 'buffer zones' which denote the regions between the sapphire windows and the commercial viewports. These buffer zones maintain good vacuum and serve as thermal insulation buffers of the conventional ICF70 flange viewports from the heated 'vapor cell' region. The strontium pieces (Aldrich, purity 99.99%, distilled dendritic pieces) are located in the vertical cylindrical part in the center. Two sapphire windows, each mounted in a copper cylinder for high thermal conductivity, confine the Sr vapor to the central 'vapor cell' region (length 60 mm). In order to avoid direct contact of the copper with Sr vapor, the copper cylinders are covered by a stainless steel plate, which also fixes the sapphire window.

The vapor cell and the buffer zones are evacuated by a 2 l/s ion getter pump via three pipes, whereby the vapor cell is pumped through a 2-mm pinhole. As a precaution, we installed water-cooled copper clamps at the ICF flange windows and the flange of the ion pump. Owing to the getter effect of Sr, a good vacuum in the buffer zones can be maintained even with no pump.

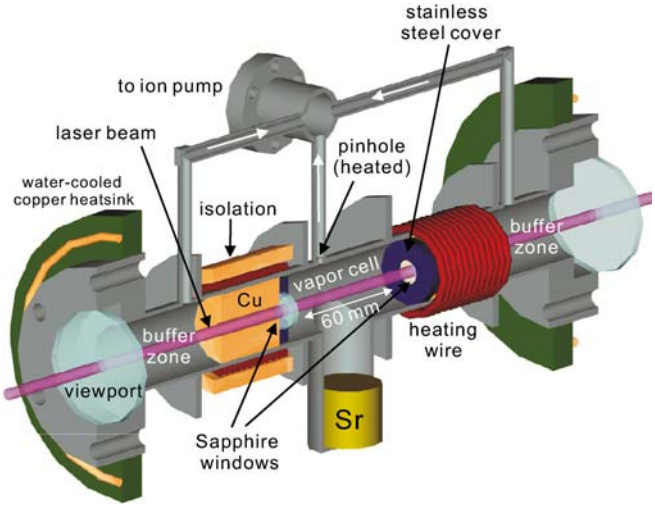

FIGURE 3 Cross section of the Sr vapor cell (in scale). Strontium vapor is confined to the central vapor cell by two sapphire windows which are heated to 520 °C. Details can be found in the text

In order to prevent condensation of Sr vapor on the sapphire windows we ensure that the windows have the highest temperature. We therefore only heat the regions of the chamber containing the windows to a temperature of 520 °C by heating wires around the UHV chamber (see Fig. 3). This results in a temperature of 360 °C (measured by a thermocouple on the chamber surface) in the region of the Sr vessel, sufficient to obtain a high-density vapor. The sapphire windows are Z-cut (optical axis in the normal direction of the surface) in order to eliminate birefringence effects. Optimum heat transfer from the chamber walls to the sapphire windows is guaranteed by their copper mount which is precisely machined as to tightly fit into the UHV chamber. The copper cylinders have drillings of 5-mm diameter at their centers for the optical path. The diameter is chosen sufficiently large to assure that transit-time broadening is small (see Sect. 2.4) without compromising the heat transfer of the copper cylinder to the sapphire windows by thermal radiation. The Doppler profile of the absorption spectrum, with maximum absorption of 15% at a laser intensity of $I = 1.6\,\mathrm{mW/cm^2}$, exhibits a line width of 750 MHz. This yields a gas temperature of $T = 400\,^{\circ}\mathrm{C}$, from which the transit-time broadening is estimated to be 25 kHz [31].

The cell has so far been operated for two years with no sign of signal reduction, demonstrating its anticipated long lifetime.

2.4 *Absolute frequency stabilization by saturation spectroscopy*

For saturation spectroscopy we employ a frequency modulation (FM) sideband technique [13]. As schematically sketched in Fig. 2, the Fabry–Pérot-stabilized laser output with FM sidebands at $f_{\mathrm{RF}} = 15.16\,\mathrm{MHz}$ is divided into a pump and a probe beam and guided to the Sr cell. In order to avoid interference effects between pump and probe beams the frequency of the pump beam is shifted by 80 MHz by an acousto-optic modulator (AOM). We define the quantization axis parallel to the polarization axis of the laser beams ($\Delta m_J = 0, \pi$ transition) applying a magnetic field of $B \approx 6\,\mathrm{mT}$ produced by a permanent magnet. As an unintentional side effect the generation of phase modulation by using an EOM is often accompanied by residual amplitude modulation (RAM) which contaminates the FM spectroscopy signal in the form of an offset drift. RAM is mainly caused by interference effects of the EOM that acts like a Fabry–Pérot etalon filled with a dielectric [33]. To eliminate this slow drift of the baseline, the pump beam is chopped at $f_{\mathrm{AF}} = 20\,\mathrm{kHz}$ using an AOM. The signal is down-converted by a double-balanced mixer (DBM) at f_{RF} and demodulated using a lock-in amplifier at f_{AF}. The result of the final demodulation is shown in Fig. 4.

The signal-to-noise ratio was 65 in a bandwidth of 10 Hz with a FWHM line width of 130 kHz. The power and the $1/e$ beam diameter of both pump and probe beams were 50 μW and 4 mm, respectively, which correspond to 50 times the saturation intensity. According to these values, the saturation broadening and the transit-time broadening [31] were estimated to be 55 kHz and 25 kHz (see Sect. 2.3), respectively. In addition, a relative misalignment of the pump and probe

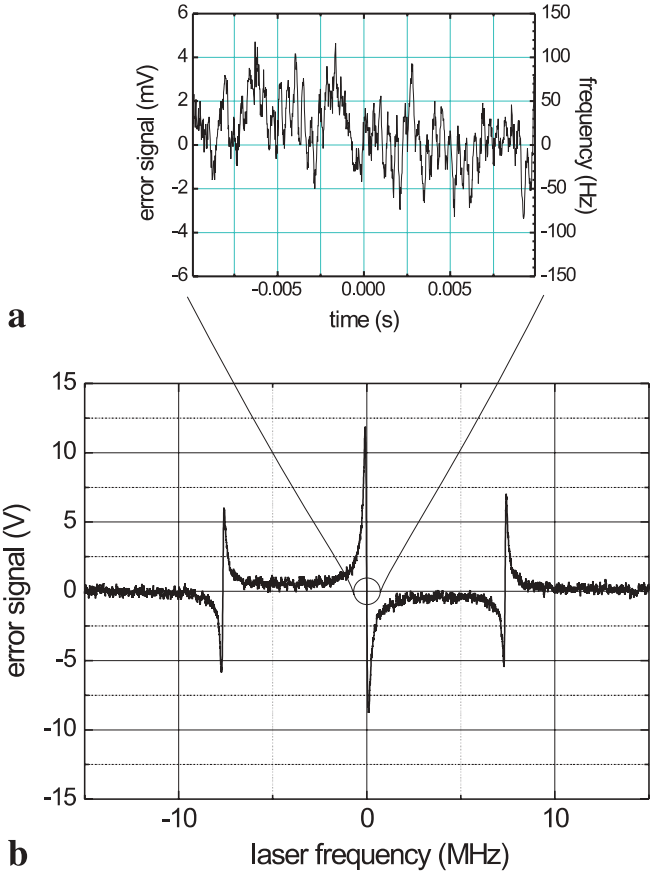

FIGURE 4 **a** Strontium saturated-absorption signal. Both pump and probe beams were frequency modulated at $f_{\mathrm{RF}} = 15.16$ MHz with an EOM and the pump beam was further square modulated at $f_{\mathrm{AF}} = 20$ kHz. The signal down converted with a double-balanced mixer at f_{RF} was lock-in detected at f_{AF}. This dispersion curve shows a strontium resonance with a 130-kHz width. We use the zero crossing of this signal as lock point for compensating the drift of the reference cavity. The correction voltage of the feedback loop is derived from the central dispersive curve. **b** The voltage fluctuation of the closed loop. The frequency fluctuation as depicted on the *right-hand axis* is converted from the error signal by the gradient of the dispersive signal near the atomic resonance

beams causes broadening due to the first-order Doppler effect. By assuming a relative misalignment of 3×10^{-4} rad, one estimates the Doppler broadening to be ~ 110 kHz.

The deviation of the frequency lock point from the true atomic resonance was measured to be less than 10 kHz by fluorescence spectroscopy of the cold atomic sample [20]. The offset is attributed mainly to the asymmetry of the saturated absorption signal and the baseline offset. Other effects which arise from collision broadening (5 kHz at a pressure of 10^{-2} Pa) [32], the recoil shift $h/2m\lambda_R^2 = 4.8$ kHz (m denotes the Sr mass), the quadratic Zeeman shift (2 kHz), and the second-order Doppler shift (1 kHz) give only negligible contributions to the line width.

2.5 *Frequency offset lock and power amplification*

In trapping experiments of the fermionic isotope ^{87}Sr with a nuclear spin of $I = 9/2$ [17], giving rise to hyperfine splitting, the frequencies for cooling and trapping are shifted by more than one GHz relative to the bosonic ^{88}Sr isotope. However, the scarce natural abundance of 7% and the Zeeman splitting into 10 sublevels in the $F = 9/2$ ground state reduce the saturated absorption signal by a factor of 100 compared to the ^{88}Sr isotope. It is therefore necessary to rely on ^{88}Sr absorption spectroscopy for ensuring frequency stability and to employ an additional 'slave' laser system which can be arbitrarily frequency shifted relative to the fixed-frequency 'master' laser system without diminishing the frequency stability. For this purpose, we implemented a heterodyne locking technique.

On the basis of the fixed-frequency master laser which is locked to the Sr reference cell, the frequency of a second 'slave' ECDL is set with an arbitrary RF frequency difference using an optical phase-locked loop (OPLL) [34] as shown in Fig. 2. A beat note between the master and slave lasers is detected by a fast photodiode and is amplified to 10 dB m level. The phase difference between the beat note and the local oscillator is demodulated by a DBM, which is then processed similarly to the stabilization of the master laser to the reference cavity. The -3 dB full line width of the stabilized beat note was measured to be less than 50 Hz, limited by the resolution of our spectrum analyzer. The bandwidth of the phase-locked loop is 2.5 MHz.

A part of the slave ECDL's beam is injected into an AR-coated laser diode and amplified to 20 mW. The amplified beam passes a double-path AOM in order to cancel beam deflection by tuning, and is guided to the trapping apparatus through a 10-m-long single-mode polarization-maintaining optical fiber, resulting in available power of 5 mW after the fiber. We checked the beat note between the beams before and after passing through the fiber, resulting in a broadened beat note of 150 Hz owing to the fiber vibration [35]. This broadening is sufficiently small compared with the line width of the transition and can therefore be neglected.

3 Resolved-sideband spectroscopy of strontium atoms in a one-dimensional optical lattice

In order to demonstrate the performance of the developed laser system, we investigated the $^1S_0$–$^3P_1$ clock transition of Sr atoms localized in the micropotentials of a one-dimensional optical lattice, where the vibrational frequencies are degenerate in the lower and upper states.

The quantum state of an atom, confined in an external potential (z direction), can be separated into the internal states and the vibrational states of the trapping potential, written as $|\,^1S_0\rangle \otimes |n\rangle$ and $|\,^3P_1\rangle \otimes |n'\rangle$ for the Sr ground and excited states, respectively (Fig. 5). Transitions can occur between these vibrational oscillator states $\{n, n'\}$ in the micropotential wells of the optical lattice, where the frequency spacing between neighboring vibrational levels is given by ν_z [36]. By appropriate choice of the lattice laser wavelength to $\lambda \approx 800$ nm and by adjusting the light polarization, the $^1S_0$ ground state and the $^3P_1$ excited state experience equal ac Stark shifts, resulting in equal vibrational frequencies ν_z in the ground and excited states, and thus leaving the atomic resonance frequency unchanged [19, 20].

In our experimental setup Sr atoms were trapped and cooled to the μK regime in a two-stage magneto-optical trap [14] and transferred into a far-off resonant optical dipole trap (FORT) configured as a one-dimensional optical lattice. The particular details of our experimental setup have been described elsewhere [20, 37]. The FORT trap beam at $\lambda \sim 800$ nm was guided in the z direction with an intensity of $P = 450$ mW. After focusing the FORT beam to a $1/e$ diameter of 90 μm the beam is reflected by a combination of a lens and a mirror in order to be re-focused at the trap center. Following the atom-loading phase, we introduce a probe beam collinear with the lattice beam and observe fluorescence photons.

The dependence of the fluorescence counts on the probe laser detuning δ_L is shown in Fig. 5. The main elastic scattering peak $|n\rangle \rightarrow |n' = n\rangle$ with FWHM 21 kHz and the first heating sideband $|n\rangle \rightarrow |n' = n+1\rangle$ are clearly resolved; their

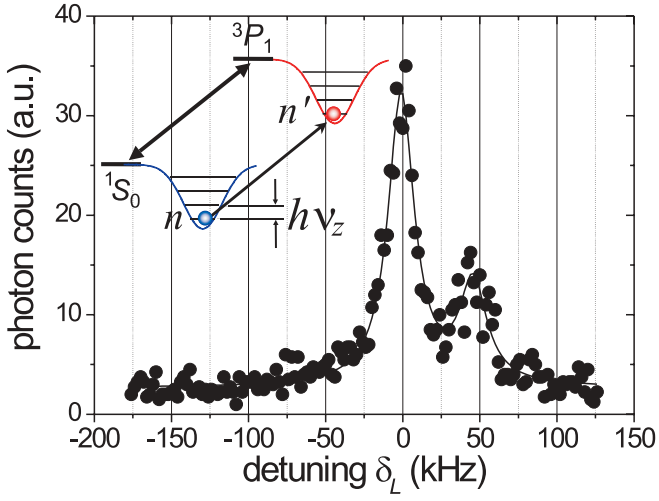

FIGURE 5 Resolved-sideband spectroscopy of Sr atoms confined in a one-dimensional optical lattice. We recorded the laser-induced fluorescence of the atoms versus the detuning δ_L of the probe beam. The elastic scattering peak at $\delta_L = 0$ and the first heating sideband at $\delta_L = +\nu_z$ are clearly resolved. The *inset* shows the position-dependent ac Stark shift produced by the FORT laser beam in the ground and the excited states. Transitions can occur between the vibrational oscillator levels of the standing wave micropotentials. A Lorentzian fit of the central elastic scattering peak gives a FWHM width of 20.7 kHz. Considering 13 kHz of saturation broadening, this signal indicates that the stability of the laser frequency was less than 16 kHz

separation suggests an oscillation frequency of $\nu_z = 50\,\mathrm{kHz}$ in the axial direction. The absence of higher-order sidebands indicates that the Lamb–Dicke condition is fulfilled.

In the data acquisition one data point was accumulated in a time of 0.4 s and averaged over 32 cycles, resulting in a total recording time of 30 min. Since the probe intensity gives a saturation line width of 13 kHz, the observed spectrum demonstrates that the long-term frequency stability of the laser is less than 16 kHz. An evaluation of further experiments [20] gives an improved estimate, yielding a line width of a few kHz in an integration time of 30 min.

4 Conclusion

We have developed a narrow-line diode laser system operating at $\lambda = 689\,\mathrm{nm}$ for trapping and cooling strontium atoms on the $^1S_0$–$^3P_1$ transition. By employing a tunable Fabry–Pérot cavity for line-width reduction and absorption spectroscopy with a heated cell of Sr vapor for establishing an absolute frequency reference, we obtained a sufficiently high frequency stability as well as good tunability for the manipulation and spectroscopy of ultra-cold Sr atoms. With the developed laser system we succeeded in confining neutral Sr atoms in a one-dimensional optical lattice and performed Doppler-free spectroscopy in the Lamb–Dicke regime.

ACKNOWLEDGEMENTS We are grateful to T. Mukaiyama for his devoted assistance to build the system and H. Hachisu for construction of the Sr heat pipe. We thank M. Kuwata-Gonokami and M. Daimon for their interest and support. T.E. acknowledges support from the Japan Society for the Promotion of Science. H.K. acknowledges financial support from the Japan Society for the Promotion of Science under a Grant-in-Aid for Young Scientists (A) KAKENHI 14702013.

REFERENCES

1 A.N. Luiten (ed.): *Frequency Measurement and Control* (Springer, Berlin 2001)
2 G. Wilpers, T. Binnewies, C. Degenhardt, U. Sterr, J. Helmcke, F. Riehle: Phys. Rev. Lett. **89**, 230 801 (2002)
3 Th. Udem, S.A. Diddams, K.R. Vogel, C.W. Oates, E.A. Curtis, W.D. Lee, W.M. Itano, R.E. Drullinger, J.C. Bergquist, L. Hollberg: Phys. Rev. Lett. **86**, 4996 (2001)
4 H. Katori: in *Proc. 6th Symp. Frequency Standards and Metrology*, ed. by P. Gill (World Scientific, Singapore 2002) pp. 323–330
5 Y. Castin, J.I. Cirac, M. Lewenstein: Phys. Rev. Lett. **80**, 5305 (1998)
6 Y. Takasu, K. Maki, K. Komori, T. Takano, K. Honda, M. Kumakura, T. Yabuzaki, Y. Takahashi: Phys. Rev. Lett. **91**, 040 404 (2003)
7 A. Derevianko, S.G. Porsev, S. Kotochigova, E. Tiesinga, P.S. Julienne: Phys. Rev. A **67**, 011 401(R) (2003)
8 S.B. Nagel, C.E. Simien, S. Laha, P. Gupta, V.S. Ashoka, T.C. Killian: Phys. Rev. Lett. **90**, 063 002-1 (2003)
9 D.P. Hansen, J.R. Mohr, A. Hemmerich: Phys. Rev. A **67**, 021 401(R) (2003)
10 F. Ruschewitz, J.L. Peng, H. Hinderthür, N. Schaffrath, K. Sengstock, W. Ertmer: Phys. Rev. Lett. **80**, 3173 (1998)
11 T. Binnewies, G. Wilpers, U. Sterr, R. Riehle, J. Helmcke, T.E. Mehlstäubler, E.M. Rasel, W. Ertmer: Phys. Rev. Lett. **87**, 123 002-1 (2001)
12 H. Wallis, W. Ertmer: J. Opt. Soc. Am. B **6**, 2211 (1989)
13 J.L. Hall, L. Hollberg, T. Baer, H.G. Robinson: Appl. Phys. Lett. **39**, 680 (1981)
14 H. Katori, T. Ido, Y. Isoya, M. Kuwata-Gonokami: Phys. Rev. Lett. **82**, 1116 (1999)
15 K.R. Vogel, T.P. Dinneen, A. Gallagher, J.L. Hall: IEEE Trans. Instrum. Meas. **48**, 618 (1999)
16 T. Kuwamoto, K. Honda, Y. Takahashi, T. Yabuzaki: Phys. Rev. A **60**, R745 (1999)
17 T. Mukaiyama, H. Katori, T. Ido, Y. Li, M. Kuwata-Gonokami: Phys. Rev. Lett. **90**, 113 002 (2003)
18 R.H. Dicke: Phys. Rev. **89**, 472 (1953)
19 H. Katori, T. Ido, M. Kuwata-Gonokami: J. Phys. Soc. Jpn. **68**, 2479 (1999)
20 T. Ido, H. Katori: Phys. Rev. Lett. **91**, 053 001 (2003)
21 F. Riehle, H. Schnatz, B. Lipphardt, G. Zinner, T. Trebst, J. Helmcke: IEEE Trans. Instrum. Meas. **48**, 613 (1999); P. Kersten, F. Mensing, U. Sterr, F. Riehle: Appl. Phys. B **68**, 27 (1999)
22 C.W. Oates, F. Bondu, R.W. Fox, L. Hollberg: Eur. Phys. J. D **7**, 449 (1999)
23 C. Wieman, L. Hollberg: Rev. Sci. Instrum. **62**, 1 (1991) and references therein
24 M.G. Littman, H.J. Metcalf: Appl. Opt. **17**, 2224 (1978)
25 K. Liu, M.G. Littman: Opt. Lett. **6**, 117 (1981)
26 R.W.P. Drever, J.L. Hall, F.V. Kowalski, J. Hough, G.M. Ford, A.J. Munley, H. Ward: Appl. Phys. B **31**, 97 (1983)
27 C.-H. Shin, M. Ohtsu: Opt. Lett. **15**, 1455 (1990)
28 J.M. Herbelin, J.A. McKay, M.A. Kwok, R.H. Uenten, D.S. Urevig, D.J. Spencer, D.J. Bernard: Appl. Opt. **19**, 144 (1980)
29 T. Kurosu, J. Ishikawa, N. Ito: Appl. Phys. B **63**, 265 (1996)
30 J.A. Neuman, P. Wang, A. Gallagher: Rev. Sci. Instrum. **66**, 3021 (1995)
31 C.J. Bordé, J.L. Hall, C.V. Kunasz, D.G. Hummer: Phys. Rev. A **14**, 236 (1976)
32 J.K. Crane, M.J. Shaw, R.W. Presta: Phys. Rev. A **49**, 1666 (1994)
33 E.A. Whittaker, M. Gehrtz, G.C. Bjorklund: J. Opt. Soc. Am. B **2**, 1320 (1985)
34 L. Ricci, M. Weidemüller, T. Esslinger, A. Hemmerich, C. Zimmermann, V. Vuletic, W. König, T.W. Hänsch: Opt. Commun. **117**, 541 (1995)
35 L.-S. Ma, P. Jungner, J. Ye, J.L. Hall: Opt. Lett. **19**, 1777 (1994)
36 F. Diedrich, J.C. Bergquist, W.M. Itano, D.J. Wineland: Phys. Rev. Lett. **62**, 403 (1989)
37 T. Ido, Y. Isoya, H. Katori: Phys. Rev. A **61**, 061403(R) (2000)